CrossMark

ARTICLE

Optical thermometry and heating based on the upconversion fluorescence from Yb^{3+}/Er^{3+} co-doped $NaLa(MoO_4)_2$ phosphor

Guofeng Liu, Zhiyi Gao, Zuoling Fu,[a] Zhen Sun, and Xiangtong Zhang
Coherent Light and Atomic and Molecular Spectroscopy Laboratory, Key Laboratory of Physics and Technology for Advanced Batteries (Ministry of Education), College of Physics, Jilin University, Changchun 130012, China

Zhijian Wu
State Key Laboratory of Rare Earth Resources Utilization, Changchun Institute of Applied Chemistry, Chinese Academy of Sciences, Changchun 130022, China

Jung Hyun Jeong[b]
Department of Physics, Pukyong National University, Busan 608-737, South Korea

(Received 10 July 2016; accepted 16 September 2016)

The $NaLa(MoO_4)_2:Yb^{3+}/Er^{3+}$ phosphor is synthesized through hydrothermal method with the further calcinations. The intense green upconversion (UC) emission is observed when it is excited by 980 nm pump power. Then we investigate the mechanism of UC emission based on the power dependent upconversion luminescence (UCL) spectra. Temperature sensing performance based on the Stark levels ($^2H_{11/2}/^4S_{3/2}$) of Er^{3+} is estimated through investigating temperature-dependent UCL spectra from 298 K to 573 K. And the maximum value of sensor sensitivity based on FIR is approximately 0.00474 K^{-1}. Moreover, the variations of UCL intensities from $^2H_{11/2}/^4S_{3/2} \rightarrow {}^4I_{15/2}$ transitions have been monitored with increasing pump power, which suggests that the pump energy can be absorbed by sample and heat it. In addition, the internal temperature of materials can be estimated by FIR technique. All the experimental results indicate that the phosphor has good potential in optical temperature sensing and optical heating.

I. INTRODUCTION

In recent years, people have paid more attention on lanthanide ion-doped phosphors for their application in remote temperature sensor and cell imaging, etc.,[1–4] which the reason is that the exist of $4f^n$ energy manifolds breaks the limit of the electric dipole selection rule. In addition, Yb^{3+}/Er^{3+} co-doped $NaLa(MoO_4)_2$ phosphor have lower phonon energy, slimmer emission bands, and longer fluorescence lifetimes, compared to conventional luminescent materials, for example, organic fluorescent dyes.[5–9]

In particular, optical thermometry is widely used in internal temperature test and electrical power stations by using the FIR technology, in which the temperature-decided UCL spectra from thermally coupled energy levels (TCLs) of rare earth ions are contributed to it.[10,11] The range of ΔE between TCLs is from 200 cm^{-1} to 2000 cm^{-1} and the quasiequilibrium is needed due to Boltzmann distribution.[12] In addition, the energy difference between the $^2H_{11/2}$ and $^4S_{3/2}$ levels of Er^{3+} is approximately 800 cm^{-1} according to previous publications, the result suggests that they have the potential to regard as an optical temperature sensor by using FIR technique.[13,14] The molybdate belongs to the sheelite-like ($CaWO_4$) iso-structure, which shows great properties for broad range of application, such as catalysts, UC material, etc.[15–18] Furthermore, the UC efficiency of molybdate is higher than traditional materials due to the lower lattice phonon energy.[19–23] So the rare earth ions-doped molybdate have ideal potential to act as an optical thermometer.

The near infrared light can be absorbed by some materials and translated into heat owing to the electron–phonon coupling, leading to the temperature of materials increasing.[13,24] In particular, the temperature rises highly when the crystal size is in nano-range. The property can be used for photothermal therapy (PTA) in medicine due to the biological tissues have little absorption for near infrared light.[25] Moreover, the internal temperature of materials and cells can be estimated by FIR of rare earth ions.[26,27]

In this paper, Yb^{3+}/Er^{3+} co-doped $NaLa(MoO_4)_2$ phosphor is prepared through hydrothermal processes.[28,29] The UCL properties of $NaLa(MoO_4)_2$ phosphor are studied in detail. And the FIR ($^2H_{11/2}/^4S_{3/2} \rightarrow {}^4I_{15/2}$ transitions) of Er^{3+} is used to investigate the optical temperature sensing from room temperature to 573 K. Then the varieties of the UCL spectra with different powers under the pump laser of 980 nm are obtained.

Contributing Editor: Winston V. Schoenfeld
Address all correspondence to these authors.
[a]e-mail: zlfu@jlu.edu.cn
[b]e-mail: jhjeong@pknu.ac.kr
DOI: 10.1557/jmr.2016.377

https://doi.org/10.1557/jmr.2016.377 Published online by Cambridge University Press

 © Materials Research Society 2016

Furthermore, the temperature of sample under different powers is calculated by FIR. The results show that the sample can be regarded as an optical temperature sensor and optical heater.

II. EXPERIMENTAL

A. Preparation of $NaLa(MoO_4)_2:Yb^{3+}/Er^{3+}$ phosphor

1. Synthesis of $NaLa(MoO_4)_2:Yb^{3+}/Er^{3+}$

The hydrothermal method was utilized to prepare the phosphor of $NaLa(MoO_4)_2$:x Er^{3+}, $y$$Yb^{3+}$ [(a) y = 5%; x = 0.5, 1, 2, 3, 4, 5, 6%; (b) x = 2%; y = 5, 10, 15%] (mole fraction).[30] All the reagents were commercially available and used without further purification. The raw materials including $(NH_4)_6Mo_7O_{24}{\cdot}4H_2O$ (99.5%, Beijing Chemical Reagent Co., Ltd), ethylene diamine tetraacetic acid (EDTA, ≥99%, Sinopharm Chemical Reagent Co., Ltd), aqueous solutions of $La(NO_3)_3$ (0.12 M), $Er(NO_3)_3$ (0.05 M), $Yb(NO_3)_3$ (0.05 M), NaOH (5 M) were obtained by dissolving lanthanide oxide and NaOH (99.99%, Shanghai Yuelong Nonferrous Metals Ltd) in dilute nitric acid solution under heating with agitation, respectively. Stoichiometric weights $La(NO_3)_3$, $Er(NO_3)_3$, and $Yb(NO_3)_3$, stoichiometric amount of $(NH_4)_6Mo_7O_{24}{\cdot}4H_2O$ and EDTA were measured and dissolved in 20 and 15 mL of deionized water to obtain solution A and solution B under stirring for 20 min and 15 min, respectively. The solution B was dropped into solution A slowly under magnetic stirring for 10 min. The value of pH was adjusted to 9 through the addition of Na(OH) (5 M) solution in the maxing solution. After stirring for half an hour, a Teflon-lined autoclave (60 mL) was needed to contain the solution and heated for 24 h at 180 °C. Then the temperature of autoclave decayed to room temperature spontaneously. The centrifugation was needed to separate the production, and the deionized water and ethanol were used to wash precursor for 3 times, then it was dehydrated 60 °C for overnight. After grinding, the precursor was burned at 800 °C for 3 h to obtain the white powder.

B. Characterization

A Rigaku-Dmax 2500 diffractometer (Rigaku Corporation, Tokyo, Japan) equipped with graphite monochromatized Cu K_α radiation (λ = 0.15405 nm) is used for measuring the x-ray diffraction (XRD), which performs the crystal structure of sample. The morphology and size of the as-obtained samples were measured by a field emission-scanning electron microscope (FE-SEM; XL30, Philips, Almelo, The Netherlands). All the results are obtained at room temperature. An Omni-λ300 spectrograph (Zolix Instruments Co. Ltd., Beijing, China) was used to detect the UCL spectra. The signal was collected by a CCD detector, which include a monochromator.

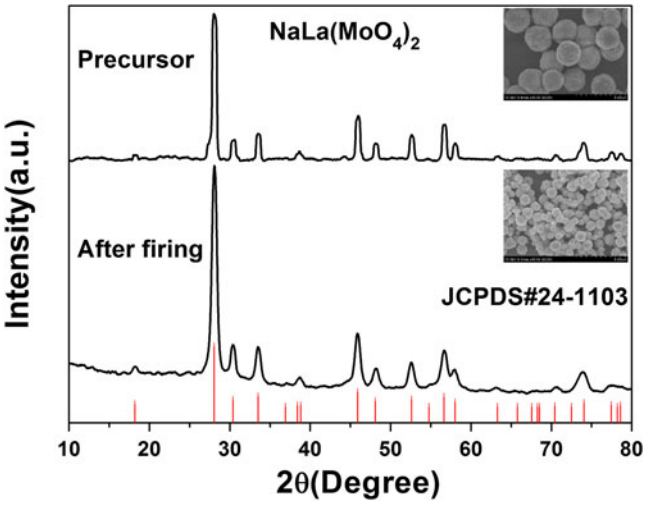


FIG. 1. XRD patterns of Yb^{3+}/Er^{3+} co-doped $NaLa(MoO_4)_2$ phosphor (precursor and phosphor after firing) at pH = 9. The standard data for $NaLa(MoO_4)_2$ (JCPDS card no. 24-11053) is shown as reference. The inset shows the FE-SEM images of precursor and phosphor after firing.

The pump source is a 980 nm diode laser, which equipped with fiber (core diameter 400 μm, numerical aperture 0.22). An Andor SR-500i spectrometer (Andor Technology Co, Belfast, UK) is used for recording the UCL spectra under the pump laser of 980 nm. The $NaLa(MoO_4)_2:Yb^{3+}/Er^{3+}$ sample is heated from 298 to 573 K in an iron sample cell. The measurement error (±1.5 K) of sample's temperature is monitored by a copper-constant thermocouple. The sample is excited in the iron sample cell by 980 nm pump power in the range of 0.036–0.797 W.

III. RESULTS AND DISCUSSION

A. The morphology and chemical characterization of $NaLa(MoO_4)_2:Yb^{3+}/Er^{3+}$ phosphor

The XRD patterns of $NaLa(MoO_4)_2:Yb^{3+}/Er^{3+}$ (precursors and after firing at 800 °C for 3 h) and the standard JCPDS card (no. 24-1103) are presented in Fig. 1. The result indicates that all the diffraction peaks of precursors and phosphors of after firing are perfectly consistent with the standard card of JCPDS (no. 24-1103), and no other impurity peaks are observed, suggesting that the sample is pure tetragonal and simultaneously Yb^{3+}/Er^{3+} ions have been entered into the host lattices. The FE-SEM images of samples are illustrated in Fig. 1. The precursors are uniformly distributed with the micro-flower morphology and the average size is around 3 μm. The phosphors of after firing are spherical in shape and the average size is about 1 μm.

B. UCL properties and energy diagram

$NaLa(MoO_4)_2$ phosphors are usually regarded as an excellent host material for its outstanding thermal and

https://doi.org/10.1557/jmr.2016.377 Published online by Cambridge University Press

hydrolytic stability.[31–34] Fig. 2 represents that the UCL intensity is a function of rare earth ion-doping concentrations under the irradiation of 980 nm laser. The spectra consist of two intense green emissions and a weak emission in the red region, which come from $^2H_{11/2}/^4S_{3/2} \rightarrow {}^4I_{15/2}$ transitions centered at 528/550 nm and $^4F_{9/2} \rightarrow {}^4I_{15/2}$ transition centered at 660 nm, respectively. In particular, the two green emissions are used to the optical temperature sensing based on FIR technique. Fig. 2(a) presents the UCL intensities of different Er^{3+} concentrations (from 0.5% to 6%) with fixed Yb^{3+} concentration (5%), the intensity rises firstly and then decreases with increasing Er^{3+} concentration in the green region due to concentration quenching effect. The intensity is highest when the Er^{3+} concentration rises to 2%. As we all know, the increase of Er^{3+} concentration leads to the shorter distance among rare earth ions, which enhances the nonradiative energy transfer. Furthermore, the UCL intensity decreases.[34] At the same time, the UCL intensities of different Yb^{3+} concentrations (from 5% to 15%) with fixed Er^{3+} concentration (2%) are shown in Fig. 2(b), and a similar situation is observed based on concentration quenching effect. The intensity is highest when the Yb^{3+} concentration is 10%. But it cannot be contributed to explain the red emission because the intensity of red emission rises with the raising Yb^{3+} concentration.[35] And the phenomenon can be explained by energy transfer (ET) from Yb^{3+} to Er^{3+}. The Yb^{3+} ions could absorb effectively 980 nm laser for its bigger absorption cross section, the ET between Yb^{3+} and Er^{3+} rises while the concentration of Yb^{3+} exceeds 10% with fixed Er^{3+} concentration, leading to the population of $^4F_{9/2}$ (Er^{3+}) level increases, and speeding up the emission from $^4F_{9/2}$ to $^4I_{15/2}$. Furthermore, the red emission enhances.[36] The insets show the digital photographs of the $NaLa(MoO_4)_2$:2%Er^{3+},5%Yb^{3+} [Fig. 2(a)] and the $NaLa(MoO_4)_2$:2%Er^{3+},10%Yb^{3+} [Fig. 2(b)]. The intense fluorescence can be observed by the naked eye under the excitation of 980 nm in the digital photographs. In addition, we can find that the green emission intensity is strong in the digital photograph of Fig. 2(a), and the red emission intensity rises in the digital photograph of Fig. 2(b) due to the raise of Yb^{3+} concentration.

Figure 3 presents the dependent UCL intensity peaks under the 980 nm pump power. The intensity of UCL increases visibly with the increasing pump power. The relation between UCL intensity and pump power can be given[37]:

$$I_{\mu p} \propto \left(P_{\text{pump}}\right)^n \quad . \tag{1}$$

where the number of infrared photons is represented by n, which can be obtained from the slope of fitting straight line, $I_{\mu p}$ notes the UCL intensity, and P_{pump} represents the pump power, respectively.[38,39] We obtain the value of n, 2.229 and 1.807 for 528 and 550 nm emissions, respectively. The result indicates that one UC photon is obtained by two infrared pumping photons in $NaLa(MoO_4)_2$:Yb^{3+}/Er^{3+} phosphor. The transitions of $^2H_{11/2}/^4S_{3/2} \rightarrow {}^4I_{15/2}$ and $^4F_{9/2} \rightarrow {}^4I_{15/2}$ can be observed under the 980 nm laser excitation. And the UC process of Er^{3+}-doped materials is investigated widely in previous reports.[40–43] Fig. 4 represents a possible UC mechanism

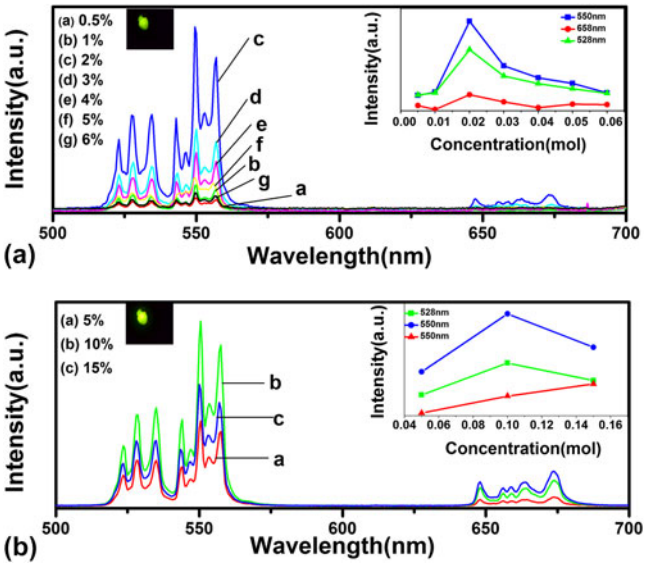


FIG. 2. Typical UCL spectra of $NaLa(MoO_4)_2$:xEr^{3+},yYb^{3+}: (a) y = 5%; x = 0.5, 1, 2, 3, 4, 5, 6% marked by (a), (b), (c), (d), (e), (f), (g), the digital photograph presents fluorescence for the $NaLa(MoO_4)_2$:5%Yb^{3+},2%Er^{3+} under the excitation of 980 nm laser; (b) x = 2%; y = 5%, 10%, 15% marked by (a), (b), (c), the digital photograph presents fluorescence for the $NaLa(MoO_4)_2$:10%Yb^{3+},2%Er^{3+} under the excitation of 980 nm laser. Insets show the normalized integrated intensities of the different peaks in the emission spectra as a function of Er^{3+} and Yb^{3+} concentrations.

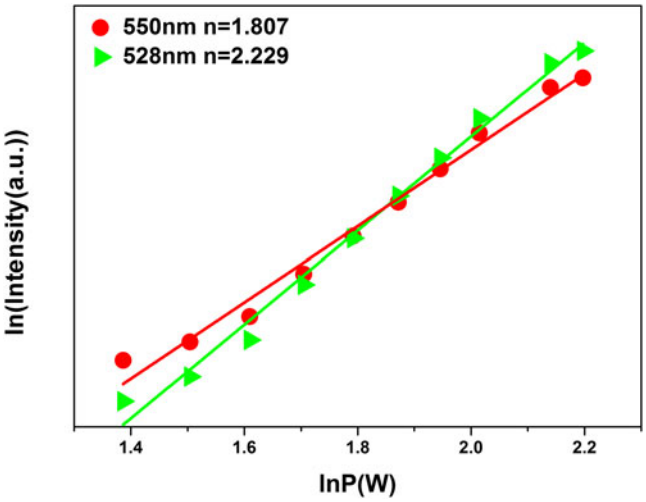


FIG. 3. The log–log plots of UCL intensity of $NaLa(MoO_4)_2$:10% Yb^{3+},2%Er^{3+} as a function of 980 nm pump power.

https://doi.org/10.1557/jmr.2016.377 Published online by Cambridge University Press

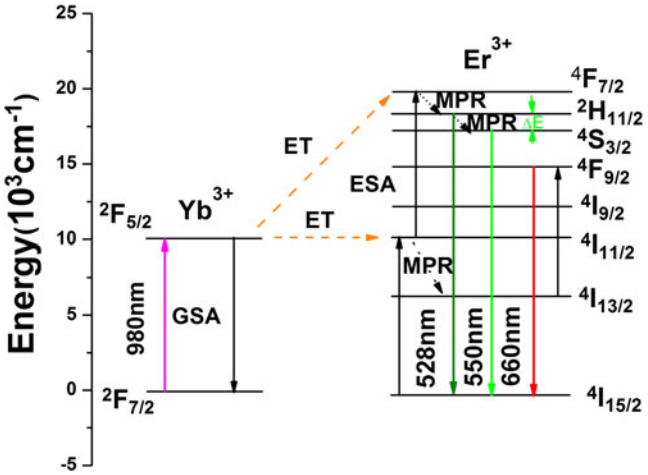


FIG. 4. The energy level diagrams of Yb^{3+}/Er^{3+} co-doped NaLa $(MoO_4)_2$ under excitation of 980 nm and possible UC processes.

for Er^{3+} ions. The population of $^2F_{7/2}(Yb^{3+})$ state can be populated to $^2F_{5/2}(Yb^{3+})$ state via the ground absorption (GSA) process. Next the population of $^4I_{15/2}(Er^{3+})$ state is populated to the metastable state $^4I_{11/2}(Er^{3+})$ based on the energy transfer (ET): $^2F_{5/2}(Yb^{3+}) + {}^4I_{15/2}(Er^{3+}) \rightarrow {}^2F_{7/2}(Yb^{3+}) + {}^4I_{11/2}(Er^{3+})$, simultaneously the population of $^2F_{5/2}$ state populates to $^2F_{7/2}$ state, then the second ET is contributed to the increase of population of $^4F_{7/2}(Er^{3+})$ state: $^2F_{5/2}(Yb^{3+}) + {}^4I_{11/2}(Er^{3+}) \rightarrow {}^2F_{7/2}(Yb^{3+}) + {}^4F_{7/2}(Er^{3+})$, simultaneously partial population of $^4I_{11/2}$ state populate to the $^4I_{13/2}$ state via a multiphonon relaxation (MPR) process and the population of $^2F_{5/2}(Yb^{3+})$ state populates to $^2F_{7/2}(Yb^{3+})$ state again. Moreover, an excited state absorption is also contributed to it: $^4I_{11/2} + h\nu \rightarrow {}^4F_{7/2}$. Then the population of $^4F_{7/2}$ state populate to $^2H_{11/2}(^4S_{3/2})$ state by a MPR process. After the first-level excitation, the population of $^4I_{13/2}$ state is populated to $^4F_{9/2}$ state under the 980 nm pump laser. Thus we can observe that the green and red emissions from $^2H_{11/2}(^4S_{3/2})$ and $^4F_{9/2}$ states to ground state, respectively.[35,43]

C. Optical temperature sensing

The Er^{3+}/Yb^{3+} co-doped $NaLa(MoO_4)_2$ phosphor is good candidate for optical temperature sensor based on thermally coupled levels (TCLs), and the UCL emission spectra are investigated. What we can find is that the FIR ($^2H_{11/2}/^4S_{3/2} \rightarrow {}^4I_{15/2}$ transitions) is proportional to the temperature. In fact, the Boltzmann law can be used to explain the population distribution of TCLs.[44,45] The population of $^4S_{3/2}$ state can be populated to the $^2H_{11/2}$ state with temperature rising via the thermalization process, leading to the intensity of $^2H_{11/2} \rightarrow {}^4I_{15/2}$ transition stronger and simultaneously the $^4S_{3/2} \rightarrow {}^4I_{15/2}$ transition weaker, which results in the FIR increasing. According to above results, the FIR from TCLs can be given as:[26,46,47]

$$\mathrm{FIR} = \frac{N_2}{N_1} = \frac{I_{2j}}{I_{1j}} = \frac{g_{2j}\sigma_{2j}\omega_{2j}}{g_{1j}\sigma_{1j}\omega_{1j}} \exp\left[\frac{-\Delta E}{K_B T}\right] = B \exp\left[\frac{-\Delta E}{K_B T}\right] \quad (2)$$

where

$$B = \frac{g_{2j}\sigma_{2j}\omega_{2j}}{g_{1j}\sigma_{1j}\omega_{1j}}$$

N notes the population of state, I represents the integrated intensity, g represents the degeneracy, σ denotes emission cross-section, and ω denotes the angular frequency. ΔE is the energy gap between the TCLs of Er^{3+} ions, K_B denotes the Boltzmann constant and T denotes the absolute temperature.[26] The evolution of FIR (I_{528}/I_{550}) with inverse absolute temperature from 298 K to 573 K on a monologue is presented in Fig. 5(a). The result shows that the data can be fitted through a straight line. And the slope is 612.2, which denotes the $\Delta E/K_B$. Figure 5(b) shows the evolution of FIR (I_{528}/I_{550}) with temperature simultaneous. Equation (2) is appropriate to fit the data and the value of B (5.36) is obtained.

It is prominent to know the change of FIR along with a certain variety of temperature for sensing application, which the sensor sensitivity of an optical thermometer could be regarded as an important reference value for it. The temperature sensitivity S is given:[48–50]

$$S = \frac{\mathrm{dFIR}}{dT} = \mathrm{FIR}\left[\frac{\Delta E}{K_B T^2}\right] = B\frac{\Delta E}{K_B T^2} \exp\left[\frac{-\Delta E}{K_B T}\right] \quad . \quad (3)$$

Equation (3) implies that broad energy gap is contributed to the increase of sensor sensitivity. What calls for special attention is that the energy gap is not too wide, otherwise there will be a lack of thermalization. Figure 6 shows the variety of $NaLa(MoO_4)_2$:Yb^{3+}/Er^{3+} sensitivity with increasing temperature. And the maximum value (0.00474 K^{-1}) is obtained at the temperature of 313 K, indicating that the sample can be used as an excellent temperature sensor, comparing to fluoride matrix, oxide, and hybrid nanoparticles.[13]

D. Analysis of thermal effect

As we all know, the excited energy can be absorbed by some material, leading to the internal temperature of material rising. And the effect of heating induced by pump laser has potential application in bio-therapy. In fact, the effect can be investigated by the fluorescence spectra in the rare earth ions doped materials, in which the calculated FIR can be used to obtain the internal temperature of material under the excitation of 980 nm pump power. Figure 7 represents the fluorescence spectra of $NaLa(MoO_4)_2$:Yb^{3+}/Er^{3+} phosphor and the inset notes the evolution of FIR (I_{528}/I_{550}) under 980 nm laser

https://doi.org/10.1557/jmr.2016.377 Published online by Cambridge University Press

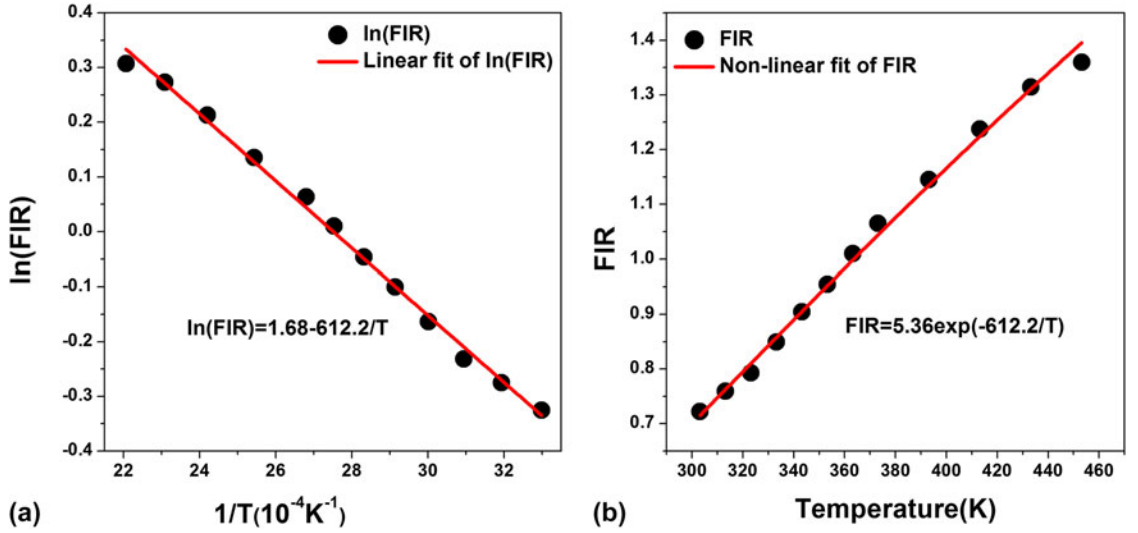


FIG. 5. (a) The monologue plot of the FIR (I_{528}/I_{550}) versus $1/T$ for the Yb^{3+}/Er^{3+} co-doped $NaLa(MoO_4)_2$ phosphor; (b) the FIR (I_{528}/I_{550}) as a function of temperature in the range of 298–573 K.

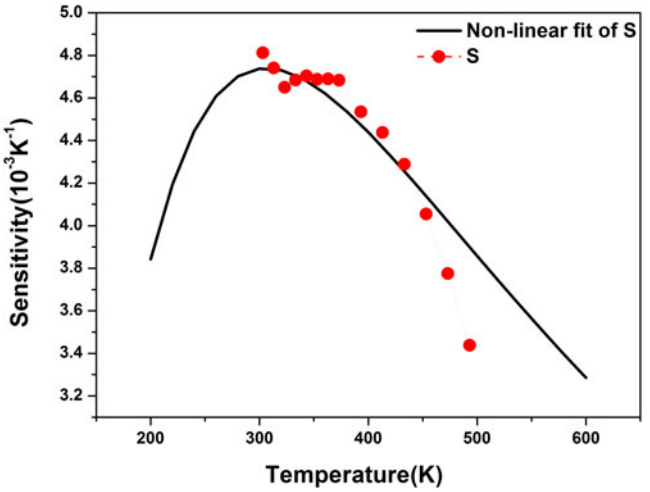


FIG. 6. The sensor sensitivity S = dFIR/dT as a function of the temperature for Yb^{3+}/Er^{3+} co-doped $NaLa(MoO_4)_2$ phosphor. S represents the value of experiment sensitivity.

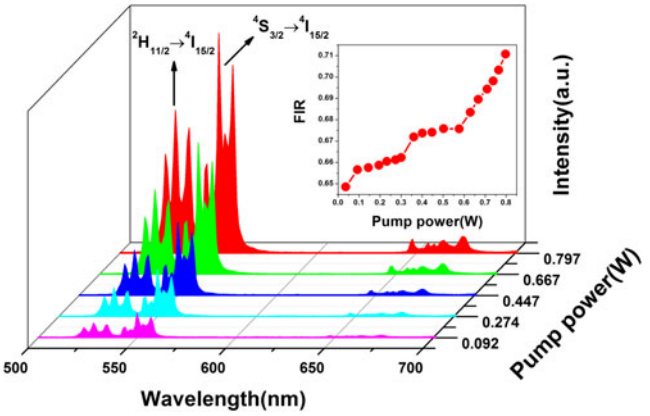


FIG. 7. The UCL spectra of the Yb^{3+}/Er^{3+} co-doped $NaLa(MoO_4)_2$ phosphors under different pumping powers. The inset represents that the FIR (I_{528}/I_{550}) as a function of laser pump power.

excitation. We can find that the luminescence intensity and FIR rise with the rise of pump power. In addition, the internal temperature of material under different pump power could be calculated by FIR, Eq. (4), which is rearranged from Eq. (2), is shown as follows[51]:

$$T = \left[\frac{1}{\ln B - \ln(\mathrm{FIR})}\right]\left[\frac{\Delta E}{K_B}\right] \quad . \qquad (4)$$

where the terms in Eq. (4) have the same meaning as Eq. (2). That the lattice temperature reaches to 302.84 K at 0.797 W. The calculated temperature of $NaLa(MoO_4)_2$: Yb^{3+}/Er^{3+} phosphor based on FIR is shown in Fig. 8. According to the above results, the crystalline nature of the material could be used to explain the phenomenon

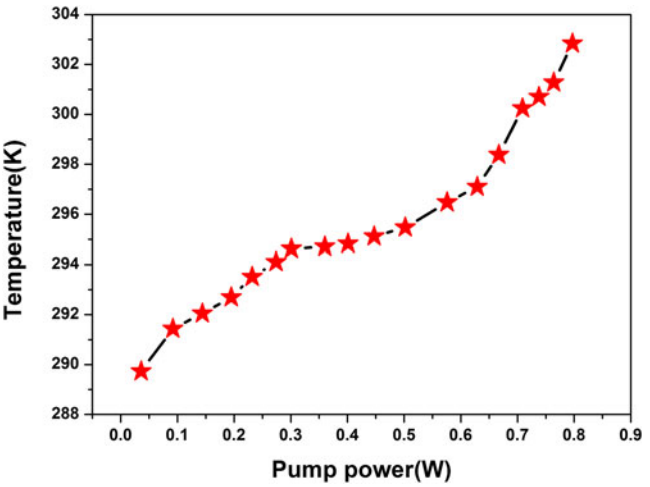


FIG. 8. Estimation of the temperature under different pump powers (980 nm) for Yb^{3+}/Er^{3+} co-doped $NaLa(MoO_4)_2$ phosphors.

https://doi.org/10.1557/jmr.2016.377 Published online by Cambridge University Press

that the temperature of the sample increases at a particular value of excitation laser and the induced heat becomes prominent by nonradiative relaxation. In general, the charged mobile carriers are driven by the laser electric field, the electrons get the infrared energy and translate it into thermal energy by the interaction between electrons and phonons. The laser induces heat transmission in the crystal by which the lattice temperature rises. The electron–phonon interactions increase in host material based on the quantum confinement of phonons, which enhances heat in the crystalline.[25,52–54]

IV. CONCLUSION

Yb^{3+} sensitized Er^{3+} doped $NaLa(MoO_4)_2$ phosphors are successfully synthesized via hydrothermal method and further calcination at 800 °C for 3 h. The UCL spectra have been investigated in different Yb^{3+} and Er^{3+} concentrations, and the UCL intensity reaches maximum value at $NaLa(MoO_4)_2$:2% Er^{3+},10% Yb^{3+} in green region. The UC spectra of material are investigated for its application in optical temperature sensing during the 298–573 K. And the maximum value of sensitivity is about 0.00474 K^{-1}, which is obtained by FIR technique. Moreover, the material can be heated by pump laser. The temperature of material induced by pump laser is estimated by the FIR technique. Above all, Yb^{3+} sensitized Er^{3+} doped $NaLa(MoO_4)_2$ phosphors can be regarded as an optical heater and temperature sensor with high sensitivity.

ACKNOWLEDGMENTS

We are grateful to the Science and Technology Development Planning Project of Jilin Province (20160101294JC), partially sponsored by China Postdoctoral Science Foundation and by the National Science Foundation of China (no. 21521092), supported by National Found for Fostering Talent of Basic Science (no. J1103202) and by the Outstanding Young Teacher Cultivation Plan in Jilin University.

REFERENCES

1. V. Muhr, S. Wilhelm, T. Hirsch, and O.S. Wolfbeis: Upconversion nanoparticles: From hydrophobic to hydrophilic surfaces. *Acc. Chem. Res.* **47**, 3481 (2014).
2. X.Q. Ge, L. Dong, L.N. Sun, Z.M. Song, R.Y. Wei, L.Y. Shi, and H.G. Chen: New nanoplatforms based on UCNPs linking with polyhedral oligomeric silsesquioxane (POSS) for multimodal bioimaging. *Nanoscale* **7**, 7206 (2016).
3. R.Y. Wei, Z.W. Wei, L.N. Sun, J.Z. Zhang, J.L. Liu, X.Q. Ge, and L.Y. Shi: Nile red derivative-modified nanostructure for upconversion luminescence sensing and intracellular detection of Fe^{3+} and MR imaging. *ACS Appl. Mater. Interfaces* **8**, 400 (2016).
4. W.B. Chen, C.J. Shi, Y. Tao, M.X. Ji, S.H. Zheng, X.W. Sang, X.F. Liu, and J.R. Qiu: Optical temperature sensing with minimized heating effect using core–shell upconversion nanoparticles. *RSC Adv.* **6**, 21540 (2016).
5. E. Matioli, S. Brinkley, K.M. Kelchner, Y.L. Hu, S. Nakamura, S. DenBaars, J. Speck, and C. Weisbuch: High-brightness polarized light-emitting diodes. *Light: Sci. Appl.* **1**, 22 (2012).
6. G.F. Wang, Q. Peng, and Y.D. Li: Upconversion luminescence of monodisperse CaF_2:Yb^{3+}/Er^{3+} nanocrystals. *J. Am. Chem. Soc.* **131**, 14200 (2009).
7. P. Li, Q. Peng, and Y.D. Li: Dual-mode luminescent colloidal spheres from monodisperse rare-earth fluoride nanocrystals. *Adv. Mater.* **21**, 1945 (2009).
8. F. Wang and X.G. Liu: Recent advances in the chemistry of lanthanide-doped upconversion nanocrystals. *Chem. Soc. Rev.* **38**, 976 (2009).
9. L.N. Sun, W.P. Mai, S. Dang, Y.N. Qiu, W. Deng, L.Y. Shi, W. Yan, and H.J. Zhang: Near-infrared luminescence of periodic mesoporous organosilicas grafted with lanthanide complexes based on visible-light sensitization. *J. Mater. Chem.* **22**, 5121 (2012).
10. X. Wang, H. Lin, D. Yang, L. Lin, and E.Y.B. Pun: Optical transitions and upconversion fluorescence in Ho^{3+}/Yb^{3+} doped bismuth tellurite glasses. *J. Appl. Phys.* **101**, 113535 (2007).
11. A.S. Gouveia-Neto, L.A. Bueno, R.F. do Nascimento, E.A. da Silva, A.B. da Costa, and V.B. do Nascimento: White light generation by frequency upconversion in $Tm^{3+}/Ho^{3+}/Yb^{3+}$-codoped fluorolead germanate glass. *Appl. Phys. Lett.* **91**, 091114 (2007).
12. L. Li, C.F. Guo, S. Jiang, D.K. Agrawal, and T. Li: Green upconversion luminescence of Yb^{3+}–Er^{3+} co-doped $CaLa_2ZnO_5$ for optically temperature sensing. *RSC Adv.* **4**, 6391 (2014).
13. Y.M. Yang, C. Mi, F. Yu, X.Y. Su, C.F. Guo, G. Li, J. Zhang, L.L. Liu, Y.Z. Liu, and X.D. Li: Optical thermometry based on the upconversion fluorescence from Yb^{3+}/Er^{3+} codoped La_2O_2S phosphor. *Ceram. Int.* **40**, 9875 (2014).
14. G.F. Liu, L.L. Fu, Z.Y. Gao, X.X. Yang, Z.L. Fu, Z.Y. Wang, and Y.M. Yang: Investigation into the temperature sensing behavior of Yb^{3+} sensitized Er^{3+} doped Y_2O_3, YAG and $LaAlO_3$ phosphors. *RSC Adv.* **5**, 51820 (2015).
15. Y. Hizhnyi, V. Chornii, S. Nedilko, M. Slobodyanik, K. Terebilenko, V. Boyko, O. Gomenyuk, and V. Sheludko: Luminescence spectroscopy of Ln-doped Bi-containing phosphates and molybdates. *Radiat. Meas.* **90**, 314 (2016).
16. E.E. Dunaeva, L.I. IvIeva, M.E. Doroshenko, P.G. Zverev, A.V. Nekhoroshikh, and V.V. Osiko: Synthesis, characterization, spectroscopy, and laser operation of $SrMoO_4$ crystals co-doped with Tm^{3+} and Ho^{3+}. *J. Cryst. Growth* **432**, 1 (2015).
17. A.M. Li, J.Z. Li, Z.Q. Chen, Y.H. Wu, L.D. Wu, G.J. Lu, C.H. Wang, and G. Zhang: Growth and spectral properties of Yb^{3+}/Ho^{3+} co-doped $NaGd(MoO_4)_{(2)}$ crystal. *Mater. Express* **5**, 527 (2015).
18. K.P. Mani, G. Vimal, P.R. Biju, C. Joseph, N.V. Unnikrishnan, and M.A. Ittyachen: Structural and spectral investigation of terbium molybdate nanophosphor. *Spectrochim. Acta. A* **148**, 412 (2015).
19. S.K. Singh, K. Kumar, and S.B. Rai: Er^{3+}/Yb^{3+} codoped Gd_2O_3 nano-phosphor for optical thermometry. *Spectrochim. Acta, Part A* **149**, 16 (2009).
20. B. Dong, D.P. Liu, X.J. Wang, T. Yang, and S.M. Miao: Optical thermometry through infrared excited green upconversion emissions in Er^{3+}–Yb^{3+} codoped Al_2O_3. *Appl. Phys. Lett.* **90**, 181117 (2007).
21. C. Li, B. Dong, S.F. Li, and C.L. Song: Er^{3+}–Yb^{3+} co-doped silicate glass for optical temperature sensor. *Chem. Phys. Lett.* **443**, 426 (2007).
22. S.Q. Zhou, C.R. Li, Z.F. Liu, S.F. Li, and C.L. Song: Thermal effect on up-conversion in Er^{3+}/Yb^{3+} co-doped silicate glass. *Opt. Mater.* **30**, 513 (2007).
23. Y.Q. Lei, H.W. Song, L.M. Yang, L.X. Yu, Z.X. Liu, G.H. Pan, X. Bai, and L.B. Fan: Upconversion luminescence, intensity

https://doi.org/10.1557/jmr.2016.377 Published online by Cambridge University Press

saturation effect, and thermal effect in $Gd_2O_3:Er^{3+},Yb^{3+}$ nanowires. *J. Chem. Phys.* **123**, 174710 (2005).
24. L.J. Zheng, X.Y. Gao, H.L. Liu, B. Li, and C.X. Xu: The heating effect of the Er^{3+}/Yb^{3+} doped Y_2O_3 nanometer powder by 980 nm laser diode pumping. *Spectrosc. Spect. Anal.* **33**, 151 (2013).
25. R.K. Verma and S.B. Rai: Laser induced optical heating from $Yb^{3+}/Ho^{3+}:Ca_{12}Al_{14}O_{33}$ and its applicability as a thermal probe. *J. Quant. Spectrosc. Radiat. Transfer* **13**, 1594 (2012).
26. J.J. Cai, X.T. Wei, F.F. Hu, Z.M. Cao, L. Zhao, Y.H. Chen, C.K. Duan, and M. Yin: Up-conversion luminescence and optical thermometry properties of transparent glass ceramics containing $CaF_2:Yb^{3+}/Er^{3+}$ nanocrystals. *Ceram. Int.* **42**, 13990 (2016).
27. R.K. Verma, A. Rai, K. Kumar, and S.B. Rai: Up and down conversion fluorescence studies on combustion synthesized $Yb^{3+}/Yb^{2+}:MO–Al_2O_3$ (M = Ca, Sr and Ba) phosphors. *J. Lumin.* **130**, 1248 (2010).
28. J.S. Liao, B. Qiu, and H.S. Lai: Synthesis and luminescence properties of $Tb^{3+}:NaGd(WO_4)_2$ novel green phosphors. *J. Lumin.* **129**, 668 (2009).
29. Y. Li, G.F. Wang, K. Pan, Y. Qu, S. Liu, and L. Feng: Formation and down/up conversion luminescence of Ln^{3+} doped $NaY(MoO_4)_2$ microcrystals. *Dalton Trans.* **42**, 3366 (2013).
30. Z.Y. Gao, Z.Y. Wang, L.L. Fu, X.X. Yang, Z.Y. Fu, Z.J. Wu, and J.H. Jeong: $NaLa(MoO_4)_2:RE^{3+}$ (RE^{3+} = Eu^{3+}, Sm^{3+}, Er^{3+}/Yb^{3+}) microspheres: The synthesis and optical properties. *Mater. Res. Bull.* **70**, 779 (2015).
31. Z.H. Xu, C.X. Li, G.G. Li, R.T. Chai, C. Peng, D.M. Yang, and J. Lin: Self-assembled 3D urchin-like $NaY(MoO_4)_2:Eu^{3+}/Tb^{3+}$ microarchitectures: Hydrothermal synthesis and tunable emission colors. *J. Phys. Chem. C* **114**, 2573 (2010).
32. S.S. Liu, D.P. Yang, D.K. Ma, S. Wang, T.D. Tang, and S.M. Huang: Single-crystal $NaY(MoO_4)_2$ thin plates with dominant facets for efficient photocatalytic degradation of dyes under visible light irradiation. *Chem. Commun.* **47**, 8013 (2011).
33. Y. Li, G.F. Wang, K. Pan, W. Zhou, C. Wang, N.Y. Fan, Y.J. Chen, Q.M. Feng, and B.B. Zhao: Controlled synthesis and luminescence properties of rhombic $NaLn(MoO_4)_2$ submicrocrystals. *Cryst. Eng. Comm* **14**, 5015 (2012).
34. L. Gomes, H.M.S.M.D. Linhares, R.U. Hmdmd Ichikawa, L.G. Martinez, and S.L. Baldochi: Luminescence properties of $Yb:Er:KY_3F_{10}$ nanophosphor and thermal treatment effects. *Opt. Mater.* **54**, 57 (2016).
35. J.H. Chung, J.H. Ryu, J.W. Eun, J.H. Lee, S.Y. Lee, T.H. Hes, B.G. Choi, and K.B. Shim: Green upconversion luminescence from poly-crystalline Yb^{3+}, Er^{3+} co-doped $CaMoO_4$. *J. Alloys Compd.* **522**, 30 (2012).
36. J. Zhang, S.W. Wang, T.J. Rong, and L.D. Chen: Upconversion luminescence in Er^{3+} doped and Yb^{3+}/Er^{3+} codoped yttria nanocrystalline powders. *J. Am. Ceram. Soc.* **87**, 1072 (2004).
37. H.D. Zeng, Z.Y. Lin, Q.A. Zhang, D.P. Chen, X.L. Liang, Y.S. Xu, and G.R. Chen: Green emission from Eu^{2+}/Dy^{3+} codoped $SrO–Al_2O_3–B_2O_3$ glass-ceramic by ultraviolet light and femtosecond laser irradiation. *Mater. Res. Bull.* **46**, 319 (2011).
38. T. Wei, Z. Dong, C.Z. Zhao, Y.J. Ma, T.B. Zhang, Y.F. Xie, Q.J. Zhou, and Z.P. Li: Up-conversion luminescence and temperature sensing properties in Er-doped ferroelectric $Sr_2Bi_4Ti_5O_{18}$. *Ceram. Int.* **42**, 5537 (2016).
39. J. Li, Z.D. Hao, X. Zhang, Y.S. Luo, J.H. Zhao, S.Z. Lu, J. Cao, and J.H. Zhang: Hydrothermal synthesis and upconversion luminescence properties of beta-$NaGdF_4:Yb^{3+}/Tm^{3+}$ and beta-$NaGdF_4:Yb^{3+}/Ho^{3+}$ submicron crystals with regular morphologies. *J. Colloid Interface Sci.* **392**, 206 (2013).
40. X.L. Li, Z.L. Xue, and H.R. Liu: Hydro-thermal synthesis of PEGylated Mn^{2+} dopant controlled $NaYF_4:Yb/Er$ up-conversion nano-particles for multi-color tuning. *J. Alloys Compd.* **681**, 379 (2016).
41. D.G. Li, W.P. Qin, T. Aidilibike, P. Zhang, S.H. Liu, L.L. Wang, and S.W. Li: Enhanced upconversion emission and magnetization in $Yb^{3+}–Er^{3+}/Ho^{3+}$ codoped Gd_2O_3 nanocrystals by introducing Zn^{2+} ions. *J. Alloys Compd.* **675**, 31 (2016).
42. F. León-Luis Sergio, U. Rodríguez-Mendozaa, R. Martína Inocencio, E. Lalla, and V. Lavín: Effects of Er^{3+} concentration on thermal sensitivity in optical temperature fluorotellurite glass sensors. *Sens. Actuators, B.* **176**, 1167 (2013).
43. R. Adhikari, J. Choi, R. Narro-García, E. DelaRosa, S. Tohru, and L. Soo Wohn: Understanding the infrared to visible upconversion luminescence properties of Er^{3+}/Yb^{3+} co-doped $BaMoO_4$ nanocrystals. *J. Solid State Chem.* **216**, 36 (2014).
44. F. Qin, H. Zhao, W. Cai, Z.G. Zhang, and W.W. Cao: A precise Boltzmann distribution law for the fluorescence intensity ratio of two thermally coupled levels. *Appl. Phys. Lett.* **108**, 241907 (2016).
45. S.A. Wade, S.F. Collins, and G.W. Baxter: Fluorescence intensity ratio technique for optical fiber point temperature sensing. *J. Appl. Phys.* **94**, 4743 (2003).
46. H.Y. Lu, H.Y. Hao, G. Shi, Y.C. Gao, R.X. Wang, Y.L. Song, Y.X. Wang, and X.R. Zhang: Optical temperature sensing in beta-$NaLuF_4:Yb^{3+}/Er^{3+}/Tm^{3+}$ based on thermal, quasi-thermal and non-thermal coupling levels. *RSC Adv.* **6**, 55307 (2016).
47. A. Kumar, S.P. Tiwari, K. Kumar, and V.K. Rai: Structural and optical properties of thermal decomposition assisted $Gd_2O_3:Ho^{3+}/Yb^{3+}$ upconversion phosphor annealed at different temperatures. *Spectrochim. Acta, Part A* **167**, 134 (2016).
48. B. Dong, B.S. Cao, and Y.Y. He: Temperature sensing and in vivo imaging by molybdenum sensitized visible upconversion luminescence of rare-earth oxides. *Adv. Mater.* **24**, 1987 (2012).
49. S.F. León-Luis, U.R. Rodríguez-Mendoza, E. Lalla, and V. Lavín: Temperature sensor based on the Er^{3+} green upconverted emission in a fluorotellurite glass. *Sens. Actuators, B* **158**, 208 (2011).
50. B.S. Cao, Y.Y. He, Z.Q. Feng, Y.S. Li, and B. Dong: Optical temperature sensing behavior of enhanced green upconversion emissions from Er-Mo: $Yb_2Ti_2O_7$ nanophosphor. *Sens. Actuators, B* **159**, 8 (2011).
51. M. Challenor, P.J. Gong, D. Lorenser, M. Fitzgerald, S. Dunlop, D.D. Sampson, and K.S. Iyer: Iron oxide-induced thermal effects on solid-state upconversion emissions in NaYF4:Yb,Er nanocrystals. *ACS Appl. Mater. Interfaces.* **5**, 7875 (2013).
52. V.K. Kikhomirov, K. Driesen, V.D. Rodriguez, P. Gredin, M. Mortier, and V.V. Moshchalkov: Optical nanoheater based on the $Yb^{3+}–Er^{3+}$ co-doped nanoparticles. *Opt. Express* **17**, 11794 (2009).
53. J. Wang, J.H. Hao, and P.A. Tanner: Luminous and tunable white-light upconversion for YAG ($Yb_3A_{15}O_{12}$) and $(Yb,Y)_2O_3$ nanopowders. *Opt. Lett.* **35**, 3922 (2010).
54. A.K. Singh, S. Singh, D. Kumar, S.B. Rai, and K. Kumar: Light-into-heat conversion in $La_2O_3:Er^{3+}–Yb^{3+}$ phosphor: An incandescent emission. *Opt. Lett.* **37**, 776 (2012).

https://doi.org/10.1557/jmr.2016.377 Published online by Cambridge University Press